Centrality and transverse-momentum dependence of higher-order flow harmonics of identified hadrons in Au+Au collisions at $\sqrt{s_{NN}} = 200$ GeV

M. S. Abdallah,[5] B. E. Aboona,[56] J. Adam,[6] L. Adamczyk,[2] J. R. Adams,[40] J. K. Adkins,[31] G. Agakishiev,[29] I. Aggarwal,[42] M. M. Aggarwal,[42] Z. Ahammed,[62] A. Aitbaev,[29] I. Alekseev,[3,36] D. M. Anderson,[56] A. Aparin,[29] E. C. Aschenauer,[6] M. U. Ashraf,[12] F. G. Atetalla,[30] G. S. Averichev,[29] V. Bairathi,[54] W. Baker,[11] J. G. Ball Cap,[21] K. Barish,[11] A. Behera,[53] R. Bellwied,[21] P. Bhagat,[28] A. Bhasin,[28] J. Bielcik,[15] J. Bielcikova,[39] I. G. Bordyuzhin,[3] J. D. Brandenburg,[6] A. V. Brandin,[36] X. Z. Cai,[51] H. Caines,[65] M. Calderón de la Barca Sánchez,[9] D. Cebra,[9] I. Chakaberia,[32] P. Chaloupka,[15] B. K. Chan,[10] F-H. Chang,[38] Z. Chang,[6] A. Chatterjee,[12] S. Chattopadhyay,[62] D. Chen,[11] J. Chen,[50] J. H. Chen,[19] X. Chen,[49] Z. Chen,[50] J. Cheng,[58] S. Choudhury,[19] W. Christie,[6] X. Chu,[6] H. J. Crawford,[8] M. Csanád,[17] M. Daugherity,[1] T. G. Dedovich,[29] I. M. Deppner,[20] A. A. Derevschikov,[44] A. Dhamija,[42] L. Di Carlo,[64] L. Didenko,[6] P. Dixit,[23] X. Dong,[32] J. L. Drachenberg,[1] E. Duckworth,[30] J. C. Dunlop,[6] J. Engelage,[8] G. Eppley,[46] S. Esumi,[59] O. Evdokimov,[13] A. Ewigleben,[33] O. Eyser,[6] R. Fatemi,[31] F. M. Fawzi,[5] S. Fazio,[7] C. J. Feng,[38] Y. Feng,[45] E. Finch,[52] Y. Fisyak,[6] A. Francisco,[65] C. Fu,[12] C. A. Gagliardi,[56] T. Galatyuk,[16] F. Geurts,[46] N. Ghimire,[55] A. Gibson,[61] K. Gopal,[24] X. Gou,[50] D. Grosnick,[61] A. Gupta,[28] W. Guryn,[6] A. Hamed,[5] Y. Han,[46] S. Harabasz,[16] M. D. Harasty,[9] J. W. Harris,[65] H. Harrison,[31] S. He,[12] W. He,[19] X. H. He,[27] Y. He,[50] S. Heppelmann,[9] S. Heppelmann,[43] N. Herrmann,[20] E. Hoffman,[21] L. Holub,[15] C. Hu,[27] Q. Hu,[27] Y. Hu,[19] H. Huang,[38] H. Z. Huang,[10] S. L. Huang,[53] T. Huang,[38] X. Huang,[58] Y. Huang,[58] T. J. Humanic,[40] D. Isenhower,[1] M. Isshiki,[59] W. W. Jacobs,[26] C. Jena,[24] A. Jentsch,[6] Y. Ji,[32] J. Jia,[6,53] K. Jiang,[49] X. Ju,[49] E. G. Judd,[8] S. Kabana,[54] M. L. Kabir,[11] S. Kagamaster,[33] D. Kalinkin,[26,6] K. Kang,[58] D. Kapukchyan,[11] K. Kauder,[6] H. W. Ke,[6] D. Keane,[30] A. Kechechyan,[29] M. Kelsey,[64] Y. V. Khyzhniak,[36] D. P. Kikoła,[63] B. Kimelman,[9] D. Kincses,[17] I. Kisel,[18] A. Kiselev,[6] A. G. Knospe,[33] H. S. Ko,[32] L. Kochenda,[36] A. Korobitsin,[29] L. K. Kosarzewski,[15] L. Kramarik,[15] P. Kravtsov,[36] L. Kumar,[42] S. Kumar,[27] R. Kunnawalkam Elayavalli,[65] J. H. Kwasizur,[26] R. Lacey,[53] S. Lan,[12] J. M. Landgraf,[6] J. Lauret,[6] A. Lebedev,[6] R. Lednicky,[29] J. H. Lee,[6] Y. H. Leung,[32] N. Lewis,[6] C. Li,[50] C. Li,[49] W. Li,[46] X. Li,[49] Y. Li,[58] X. Liang,[11] Y. Liang,[30] R. Licenik,[39] T. Lin,[50] Y. Lin,[12] M. A. Lisa,[40] F. Liu,[12] H. Liu,[26] H. Liu,[12] P. Liu,[53] T. Liu,[65] X. Liu,[40] Y. Liu,[56] Z. Liu,[49] T. Ljubicic,[6] W. J. Llope,[64] R. S. Longacre,[6] E. Loyd,[11] T. Lu,[27] N. S. Lukow,[55] X. F. Luo,[12] L. Ma,[19] R. Ma,[6] Y. G. Ma,[19] N. Magdy,[13] D. Mallick,[37] S. L. Manukhov,[29] S. Margetis,[30] C. Markert,[57] H. S. Matis,[32] J. A. Mazer,[47] N. G. Minaev,[44] S. Mioduszewski,[56] B. Mohanty,[37] M. M. Mondal,[53] I. Mooney,[64] D. A. Morozov,[44] A. Mukherjee,[17] M. Nagy,[17] J. D. Nam,[55] Md. Nasim,[23] K. Nayak,[12] D. Neff,[10] J. M. Nelson,[8] D. B. Nemes,[65] M. Nie,[50] G. Nigmatkulov,[36] T. Niida,[59] R. Nishitani,[59] L. V. Nogach,[44] T. Nonaka,[59] A. S. Nunes,[6] G. Odyniec,[32] A. Ogawa,[6] S. Oh,[32] V. A. Okorokov,[36] K. Okubo,[59] B. S. Page,[6] R. Pak,[6] J. Pan,[56] A. Pandav,[37] A. K. Pandey,[59] Y. Panebratsev,[29] P. Parfenov,[36] A. Paul,[11] B. Pawlik,[41] D. Pawlowska,[63] C. Perkins,[8] J. Pluta,[63] B. R. Pokhrel,[55] J. Porter,[32] M. Posik,[55] V. Prozorova,[15] N. K. Pruthi,[42] M. Przybycien,[2] J. Putschke,[64] H. Qiu,[27] A. Quintero,[55] C. Racz,[11] S. K. Radhakrishnan,[30] N. Raha,[64] R. L. Ray,[57] R. Reed,[33] H. G. Ritter,[32] M. Robotkova,[39] O. V. Rogachevskiy,[29] J. L. Romero,[9] D. Roy,[47] L. Ruan,[6] A. K. Sahoo,[23] N. R. Sahoo,[50] H. Sako,[59] S. Salur,[47] E. Samigullin,[3] J. Sandweiss,[65,*] S. Sato,[59] A. M. Schmah,[32] W. B. Schmidke,[6] N. Schmitz,[34] B. R. Schweid,[53] F. Seck,[16] J. Seger,[14] R. Seto,[11] P. Seyboth,[34] N. Shah,[25] E. Shahaliev,[29] P. V. Shanmuganathan,[6] M. Shao,[49] T. Shao,[19] R. Sharma,[24] A. I. Sheikh,[30] D. Y. Shen,[19] S. S. Shi,[12] Y. Shi,[50] Q. Y. Shou,[19] E. P. Sichtermann,[32] R. Sikora,[2] J. Singh,[42] S. Singha,[27] P. Sinha,[24] M. J. Skoby,[45] N. Smirnov,[65] Y. Söhngen,[20] W. Solyst,[26] Y. Song,[65] H. M. Spinka,[4,*] B. Srivastava,[45] T. D. S. Stanislaus,[61] M. Stefaniak,[63] D. J. Stewart,[65] M. Strikhanov,[36] B. Stringfellow,[45] A. A. P. Suaide,[48] M. Sumbera,[39] B. Summa,[43] X. M. Sun,[12] X. Sun,[13] Y. Sun,[49] Y. Sun,[22] B. Surrow,[55] D. N. Svirida,[3] Z. W. Sweger,[9] P. Szymanski,[63] A. H. Tang,[6] Z. Tang,[49] A. Taranenko,[36] T. Tarnowsky,[35] J. H. Thomas,[32] A. R. Timmins,[21] D. Tlusty,[14] T. Todoroki,[59] M. Tokarev,[29] C. A. Tomkiel,[33] S. Trentalange,[10] R. E. Tribble,[56] P. Tribedy,[6] S. K. Tripathy,[17] T. Truhlar,[15] B. A. Trzeciak,[15] O. D. Tsai,[10] Z. Tu,[6] T. Ullrich,[6] D. G. Underwood,[4,61] I. Upsal,[46] G. Van Buren,[6] J. Vanek,[39] A. N. Vasiliev,[44,36] I. Vassiliev,[18] V. Verkest,[64] F. Videbæk,[6] S. Vokal,[29] S. A. Voloshin,[64] F. Wang,[45] G. Wang,[10] J. S. Wang,[22] P. Wang,[49] X. Wang,[50] Y. Wang,[12] Y. Wang,[58] Z. Wang,[50] J. C. Webb,[6] P. C. Weidenkaff,[20] G. D. Westfall,[35] H. Wieman,[32] S. W. Wissink,[26] R. Witt,[60] J. Wu,[12] J. Wu,[27] Y. Wu,[11] B. Xi,[51] Z. G. Xiao,[58] G. Xie,[32] W. Xie,[45] H. Xu,[22] N. Xu,[32] Q. H. Xu,[50] Y. Xu,[50] Z. Xu,[6] Z. Xu,[10] G. Yan,[50] C. Yang,[50] Q. Yang,[50] S. Yang,[46] Y. Yang,[38] Z. Ye,[46] Z. Ye,[13] L. Yi,[50] K. Yip,[6] Y. Yu,[50] H. Zbroszczyk,[63] W. Zha,[49] C. Zhang,[53] D. Zhang,[12] J. Zhang,[50] S. Zhang,[13] S. Zhang,[19] Y. Zhang,[27] Y. Zhang,[49] Y. Zhang,[12] Z. J. Zhang,[38] Z. Zhang,[6] Z. Zhang,[13] F. Zhao,[27] J. Zhao,[19] M. Zhao,[6] C. Zhou,[19] Y. Zhou,[12] X. Zhu,[58] M. Zurek,[4] and M. Zyzak[18]

(STAR Collaboration)

[1]*Abilene Christian University, Abilene, Texas 79699*

[2]*AGH University of Science and Technology, FPACS, Cracow 30-059, Poland*

[3]*Alikhanov Institute for Theoretical and Experimental Physics NRC "Kurchatov Institute", Moscow 117218*

[4]*Argonne National Laboratory, Argonne, Illinois 60439*

[*]Deceased.

[5]*American University of Cairo, New Cairo 11835, New Cairo, Egypt*
[6]*Brookhaven National Laboratory, Upton, New York 11973*
[7]*University of Calabria & INFN-Cosenza, Italy*
[8]*University of California, Berkeley, California 94720*
[9]*University of California, Davis, California 95616*
[10]*University of California, Los Angeles, California 90095*
[11]*University of California, Riverside, California 92521*
[12]*Central China Normal University, Wuhan, Hubei 430079*
[13]*University of Illinois at Chicago, Chicago, Illinois 60607*
[14]*Creighton University, Omaha, Nebraska 68178*
[15]*Czech Technical University in Prague, FNSPE, Prague 115 19, Czech Republic*
[16]*Technische Universität Darmstadt, Darmstadt 64289, Germany*
[17]*ELTE Eötvös Loránd University, Budapest H-1117, Hungary*
[18]*Frankfurt Institute for Advanced Studies FIAS, Frankfurt 60438, Germany*
[19]*Fudan University, Shanghai, 200433*
[20]*University of Heidelberg, Heidelberg 69120, Germany*
[21]*University of Houston, Houston, Texas 77204*
[22]*Huzhou University, Huzhou, Zhejiang 313000*
[23]*Indian Institute of Science Education and Research (IISER), Berhampur 760010, India*
[24]*Indian Institute of Science Education and Research (IISER) Tirupati, Tirupati 517507, India*
[25]*Indian Institute Technology, Patna, Bihar 801106, India*
[26]*Indiana University, Bloomington, Indiana 47408*
[27]*Institute of Modern Physics, Chinese Academy of Sciences, Lanzhou, Gansu 730000*
[28]*University of Jammu, Jammu 180001, India*
[29]*Joint Institute for Nuclear Research, Dubna 141 980*
[30]*Kent State University, Kent, Ohio 44242*
[31]*University of Kentucky, Lexington, Kentucky 40506-0055*
[32]*Lawrence Berkeley National Laboratory, Berkeley, California 94720*
[33]*Lehigh University, Bethlehem, Pennsylvania 18015*
[34]*Max-Planck-Institut für Physik, Munich 80805, Germany*
[35]*Michigan State University, East Lansing, Michigan 48824*
[36]*National Research Nuclear University MEPhI, Moscow 115409*
[37]*National Institute of Science Education and Research, HBNI, Jatni 752050, India*
[38]*National Cheng Kung University, Tainan 70101*
[39]*Nuclear Physics Institute of the CAS, Rez 250 68, Czech Republic*
[40]*Ohio State University, Columbus, Ohio 43210*
[41]*Institute of Nuclear Physics PAN, Cracow 31-342, Poland*
[42]*Panjab University, Chandigarh 160014, India*
[43]*Pennsylvania State University, University Park, Pennsylvania 16802*
[44]*NRC "Kurchatov Institute", Institute of High Energy Physics, Protvino 142281*
[45]*Purdue University, West Lafayette, Indiana 47907*
[46]*Rice University, Houston, Texas 77251*
[47]*Rutgers University, Piscataway, New Jersey 08854*
[48]*Universidade de São Paulo, São Paulo 05314-970, Brazil*
[49]*University of Science and Technology of China, Hefei, Anhui 230026*
[50]*Shandong University, Qingdao, Shandong 266237*
[51]*Shanghai Institute of Applied Physics, Chinese Academy of Sciences, Shanghai 201800*
[52]*Southern Connecticut State University, New Haven, Connecticut 06515*
[53]*State University of New York, Stony Brook, New York 11794*
[54]*Instituto de Alta Investigación, Universidad de Tarapacá, Arica 1000000, Chile*
[55]*Temple University, Philadelphia, Pennsylvania 19122*
[56]*Texas A&M University, College Station, Texas 77843*
[57]*University of Texas, Austin, Texas 78712*
[58]*Tsinghua University, Beijing 100084*
[59]*University of Tsukuba, Tsukuba, Ibaraki 305-8571, Japan*
[60]*United States Naval Academy, Annapolis, Maryland 21402*
[61]*Valparaiso University, Valparaiso, Indiana 46383*
[62]*Variable Energy Cyclotron Centre, Kolkata 700064, India*
[63]*Warsaw University of Technology, Warsaw 00-661, Poland*

[64]*Wayne State University, Detroit, Michigan 48201*
[65]*Yale University, New Haven, Connecticut 06520*

(Received 14 March 2022; accepted 6 June 2022; published 27 June 2022)

We present high-precision measurements of elliptic, triangular, and quadrangular flow v_2, v_3, and v_4, respectively, at midrapidity for identified hadrons π, p, K, φ, K_s, Λ as a function of centrality and transverse momentum in Au+Au collisions at the center-of-mass energy $\sqrt{s_{NN}} = 200$ GeV. We observe similar v_n trends between light and strange mesons which indicates that the heavier strange quarks flow as strongly as the lighter up and down quarks. The number-of-constituent-quark scaling for v_2, v_3, and v_4 is found to hold within statistical uncertainty for 0–10%, 10–40%, and 40–80% collision centrality intervals. The results are compared to several viscous hydrodynamic calculations with varying initial conditions, and could serve as an additional constraint to the development of hydrodynamic models.

DOI: 10.1103/PhysRevC.105.064911

I. INTRODUCTION

A main goal of high-energy heavy-ion facilities such as the Relativistic Heavy-Ion Collider (RHIC) and the Large Hadron Collider (LHC) is to understand the properties of the quark-gluon plasma (QGP) [1–3]. Of particular importance are the transport properties of the QGP, especially the specific shear viscosity per unit of entropy density, (η/s), which describes the ability of the QGP to transport and dissipate momentum. Anisotropic flow measurements quantify the azimuthal anisotropy of the particle emission in the transverse plane. These reflect the viscous hydrodynamic response to the initial spatial distribution of energy density produced in the early stages of the collision [4–27].

Experimentally, anisotropic flow can be characterized using the Fourier expansion [28,29] of the azimuthal distribution as [29]

$$E\frac{d^3N}{d^3p} = \frac{1}{2\pi}\frac{d^2N}{p_T dp_T dy}\left(1 + \sum_{i=1}^{N} 2v_n \cos\left[n(\phi - \psi_{RP})\right]\right), \tag{1}$$

where v_n is the nth-order flow coefficient, E is the energy, p_T is transverse momentum, y is rapidity, ϕ is the particle azimuthal angle, and ψ_{RP} is the azimuth of the reaction plane given by the beam direction and impact parameter. The first, second, third, and fourth Fourier harmonics (v_1, v_2, v_3, and v_4) are called the directed flow, elliptic flow [28,29], triangular flow, and quadrangular flow, respectively.

Previous measurements of identified hadrons by the STAR Collaboration [30–34] were limited to the elliptic flow v_2 and little information was shown about the higher-order flow harmonics v_n with $n > 2$. Those $v_2(p_T)$ ($p_T = \sqrt{p_x^2 + p_y^2}$) measurements showed mass-order dependence (i.e., the $v_2(p_T)$ dependence on the particle species) [35] at low p_T, $p_T < 2.0$ GeV/c, which is understood to result from the hydrodynamic expansion of the medium [36]. For the intermediate-p_T region, $2.0 < p_T < 4.0$ GeV/c, the identified hadron $v_2(p_T)$ magnitudes are larger for baryons than mesons (which is referred to as baryon-meson splitting). Such an observation can be described by quark coalescence models [37–39]. In the quark coalescence picture, partons develop flow during the partonic evolution and the hadron flow is given by the sum of the collective flow of the constituent partons. The quark coalescence mechanism explains the observed number-of-constituent-quark (NCQ) scaling of $v_2(p_T)$ at RHIC.

In this paper, we extend the prior measurements by adding results on v_3 and v_4 of identified hadrons π, p, K, φ, K_s, Λ for Au+Au collisions at $\sqrt{s_{NN}} = 200$ GeV as a function of both transverse momentum (p_T) and centrality. Due to the strong viscous effects on the higher-order anisotropic flow coefficients v_n with $n > 2$, higher-order harmonics $v_{n>2}$ are expected to be more sensitive to η/s than the elliptic flow v_2 [18,40]. In addition, previous studies indicate that NCQ scaling (n_q is the number of constituent quarks) works well for the elliptic flow v_2, but does not for the higher harmonics [41,42]. As proposed in Ref. [43], a modified form of the scaling function, $v_n/n_q^{n/2}$, is tested here. It works better for v_3 and v_4 up to the intermediate-p_T region [30,44–49]. Although hadronic rescattering might be treated as a reason of the modification in scaling, the underlying physics is under discussion [50,51].

The present measurements will not only supplement other anisotropic flow studies of identified particles for Pb+Pb collisions at the LHC energies as reported in Refs [42,52,53], but also be compared to two hydrodynamic models [54,55], which are summarized in Table I. The first, Hydro-1 [54], employs the TRENTO model [56] initial state and does not include a hadronic afterburner. The second, Hydro-2 [55], uses an IP-Glasma [57] initial state in conjunction with a UrQMD [58,59] afterburner. Hydro-II also imposes the effects of global momentum and local charge conservation.

This paper is organized as follows. Section II describes the experimental setup. In Sec. III, the particle identification, the event plane reconstruction, v_n signal extraction, and systematic uncertainty estimation are discussed. In Sec. IV, the centrality and momentum dependent v_n results are presented and discussed. The summary is presented in Sec. V.

II. EXPERIMENTAL SETUP

The Solenoidal Tracker At RHIC (STAR) at the Brookhaven National Laboratory employs a solenoidal magnet and multiple detectors to provide a wide-acceptance measurement at midrapidity [60]. In this analysis, the primary

TABLE I. Summary of the two hydrodynamic models Hydro-1 [54] and Hydro-2 [55].

	Hydro-1 [54]	Hydro-2 [55]
η/s	0.05	0.12
Initial conditions	TRENTO	IP-Glasma
Contributions	Hydro + direct decays	Hydro + hadronic cascade

detectors used were the STAR Time-Projection Chamber (TPC) and the time-of-flight (ToF) systems.

The TPC has a pseudorapidity, η, acceptance of $|\eta| < 1.8$, and full azimuthal coverage [61]. Along the beam direction, the central membrane divides the TPC into two halves. Within the TPC radius of $0.5 < r < 2$ m, tracks can be reconstructed with a maximum of 45 hit points per track. The specific energy loss (dE/dx) provided by the TPC for each reconstructed track can be used for particle identification. The time-of-flight detector is based on multigap resistive plate chambers (MRPCs) [62]. The ToF detector has a time resolution of ≈ 85 ps, and covers the full azimuth and a pseudorapidity range of $|\eta| < 0.94$. The particle mass squared, m^2, provided by the ToF system significantly extends STAR's particle identification capabilities to higher p_T. Additional details on the use of these detectors are provided in Sec. III A.

The Au+Au 200 GeV data collected in the year 2011 with about 4×10^8 events is used in this analysis. A minimum bias trigger based on a coincidence of the signals from the zero degree calorimeters (ZDCs) [63], vertex position detectors (VPDs) [64], and/or beam-beam bounters (BBCs) [60] was used. Collisions more than ± 30 cm from the center of STAR along the beam direction, or more than 2 cm radially from the center of the beam pipe, were rejected. The absolute difference between the z-vertex positions measured by the TPC and VPD detectors in each event was required to be less than 3 cm to reduce background events. Collision centrality is inferred from the measured event-by-event multiplicity with the aid of a Monte Carlo Glauber simulation [65,66]. Also, a multivariate quality assurance of each data-taking run was performed. The values of the mean transverse momentum, the mean vertex position, and the mean multiplicity in the detector in single data-taking runs were all required to be within 3σ away of their mean values over the entire data set. Track quality cuts were applied to suppress backgrounds and to improve the resolution of track quantities such as the momentum and energy loss. Each track was required to have at least 15 hits assigned to it (out of up to 45). In order to remove track splitting the ratio of the number of reconstructed hits to the maximum possible number of hits for each track was required to be larger than 0.51. Tracks with $|\eta| > 0.9$ and momenta below 0.2 GeV/c, or above 4.0 GeV/c, were rejected.

III. METHODOLOGY

A. Particle identification

Particle identification (PID) in the STAR experiment can be done in multiple ways [41]. The identification of charged particles is based on a combination of momentum information, the specific energy loss dE/dx in the TPC, and a required time-of-flight measurement with the ToF detector. Charged pions and kaons can be easily distinguished on the basis of their dE/dx values for momenta up to approximately 0.7 GeV/c; at higher momenta the particles' dE/dx distributions overlap. At higher momenta, two-dimensional fits in a combined m^2 vs dE/dx plane were used to statistically extract the particle yield for π and K [41]. Protons and antiprotons are identified mainly by the time-of-flight m^2 information. To suppress contributions from pions and kaons an additional cut on $|n\sigma_p| < 2.5$ was applied. At low transverse momenta ($p_T < 2$ GeV/c) the separation of protons relative to pions and kaons is good enough to count all protons within an equivalent range of 3σ around the center of the $n\sigma_p$ distribution. At high p_T the tails on the left of the proton distributions are excluded to avoid contamination from pions and kaons. Thus the m^2 cut value increases with p_T.

The unstable particles K^0_s, φ, Λ, and $\bar{\Lambda}$ decay into a pair of oppositely charged particles and can be reconstructed using the invariant mass technique. For weak decay particles, additional topological constraints on the decay kinematics were applied to suppress backgrounds. The combinatorial background from uncorrelated particles was reduced by employing cuts on the daughter particle dE/dx and/or m^2, as well as on the topology of the specific decay. The misidentification of the daughter particles, which is more probable at higher momenta, can result in an additional correlated background. Such a correlated background, for example from the Λ hyperon, can appear in the $\pi^+\pi^-(K^0_S)$ invariant mass distribution if the proton was misidentified as a π^+. Such a correlated background does not create a peak in the invariant mass distribution of the particles of interest because the daughter-particle masses are assumed to be the nominal ones (e.g., π mass instead of proton mass), but instead appears as a broad distribution which can significantly affect the signal extraction. This correlated background can be eliminated by investigating additional invariant mass spectra with identical track combinations, but different daughter mass values. The background was removed by applying invariant mass cuts on the corresponding unwanted peaks in the misidentified invariant mass distributions. Usually, the correlated background from particle misidentification increases with the p_T values of the mother particle. In this work, the remaining uncorrelated combinatorial background was subtracted with the mixed-event technique.

B. v_n Analysis method

In this work we used the two-particle cumulant method to extract the flow coefficients v_n of π, K, and p. For other particles we used the event plane (EP) method to measure the v_2 and v_3 values. In this section, a description of each method used here is provided.

1. Two-particle cumulant method

The framework for the cumulant method is described in Refs. [67,68], which was extended to the case of subevents in Refs. [69,70]. The two-particle correlations were constructed using the two-subevent cumulant method [70], with particle

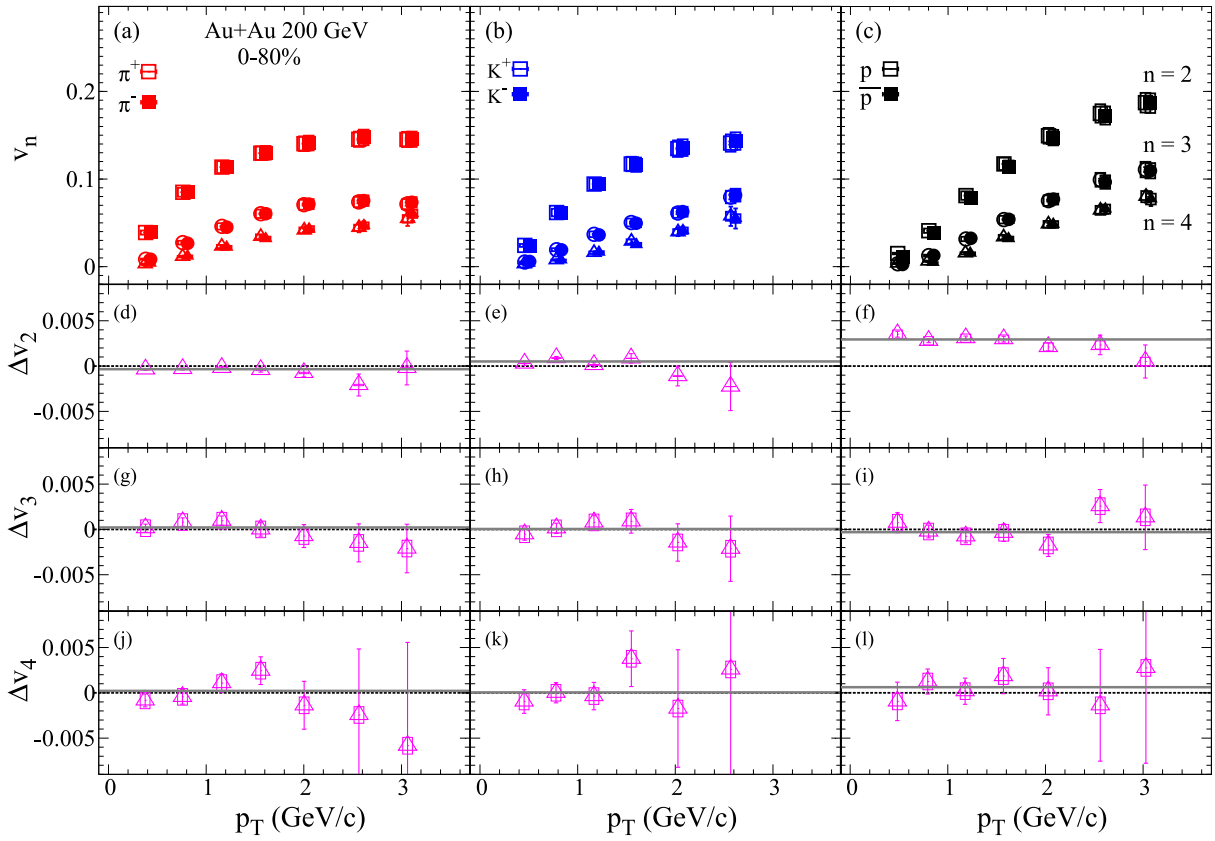

FIG. 1. The panels (a)–(c) show the transverse-momentum dependence of elliptic, triangular, and quadrangular flow of particles and antiparticles for 0–80% central Au+Au collisions at $\sqrt{s_{NN}} = 200$ GeV using the two-particle cumulant method. The panels (d)–(l) represent the v_2, v_3, and v_4 differences between positive and negative particles. Solid lines are linear fits to the data.

weights, e.g., weighted with the particle acceptance correction, and $\Delta\eta > 0.7$ separation between the subevents A and B (i.e., $1 > \eta_A > 0.35$ and $-1 < \eta_B < -0.35$). The use of the two-subevent method reduces the nonflow correlations including the decay of resonances to several charged daughter particles, Hanbury-Brown–Twiss correlations, and jets [47]. The two-particle flow harmonics can be written as

$$v_n^2 = \langle\langle \cos\left(n\left[\varphi_i^A - \varphi_j^B\right]\right)\rangle\rangle, \tag{2}$$

where $\langle\langle\,\rangle\rangle$ indicates the average over all particles in a single event and over all events, and φ_i is the azimuthal angle of the ith particle. The integrated and p_T differential nth-order flow harmonics are given as

$$v_n = \langle\langle \cos\left(n\left[\varphi_i^A - \varphi_j^B\right]\right)\rangle\rangle / \sqrt{v_n^2} \tag{3}$$

and

$$v_n(p_T, \mathrm{PID}) = \langle\langle \cos\left(n\left[\varphi_i^A(p_T, \mathrm{PID}) - \varphi_j^B\right]\right)\rangle\rangle / \sqrt{v_n^2}. \tag{4}$$

2. *Event plane method*

The nth-order event planes, Ψ_n, used here are constructed from the azimuthal distribution of final-state particles [29] as

$$\Psi_n = \tan^{-1}\left(\frac{\sum_i w_i \sin(n\varphi_i)}{\sum_i w_i \cos(n\varphi_i)}\right) \Big/ n \tag{5}$$

where φ_i is the azimuthal angle of ith particle and w_i is its weight that reflect the detector η-ϕ acceptance correction. Only tracks with momentum in the range from 0.2 to 2 GeV/c and pseudorapidity $|\eta| < 1$ in the TPC were used to calculate the event plane(s).

Two planes (east and west) are constructed using tracks from the opposite pseudorapidity hemisphere to the particle of interest, i.e., the east η_{sub} event plane using tracks with $-1.0 \leqslant \eta \leqslant -0.05$ and the west η_{sub} event plane using tracks with $0.05 \leqslant \eta \leqslant 1.0$. This procedure is called the "η-sub" method and suppresses the nonflow contribution [47]. The additional bias in the event plane reconstruction caused by detector inefficiencies generates a nonuniform Ψ_n angle distribution in the laboratory coordinate system. To flatten this distribution, the recentering [71] and shifting [72] method were applied. The event plane resolution was calculated from the two η-sub events [47]. Each of the flow harmonics was measured with respect to the corresponding, same-order, event plane.

C. Systematic uncertainty analysis

The systematic uncertainties associated with the measurements shown in this paper are evaluated by varying several parameters of the analysis and comparing the measurements with their nominal values. The systematic uncertainty correlated with the event selection is evaluated by studying the variation of the results with different selections on the primary

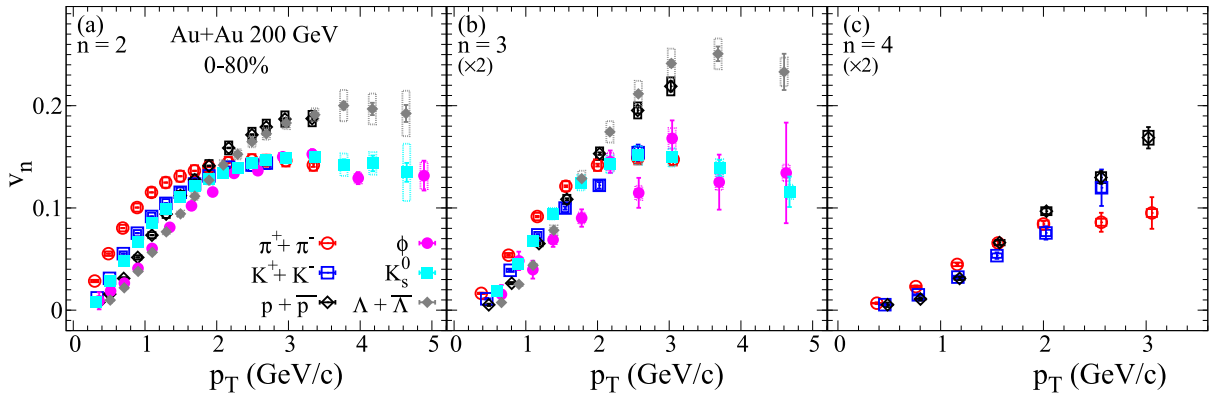

FIG. 2. The transverse-momentum dependence of the identified particle v_2 (a), v_3 (b), and v_4 (c) for 0–80% central Au+Au collisions at $\sqrt{s_{NN}} = 200$ GeV.

vertex position, i.e., using a range −30 to 0 cm or 0 to 30 cm rather than the nominal range of ±30 cm. The event-cuts systematic uncertainty ranges from 1% to 2% from central to peripheral collisions. The systematic uncertainty resulting from the track selection is estimated by applying stricter conditions: (i) distance of closest approach (DCA) is reduced to be less than 2 cm rather than 3 cm, and (ii) the number of TPC space points changing from more than 15 points to more than 20

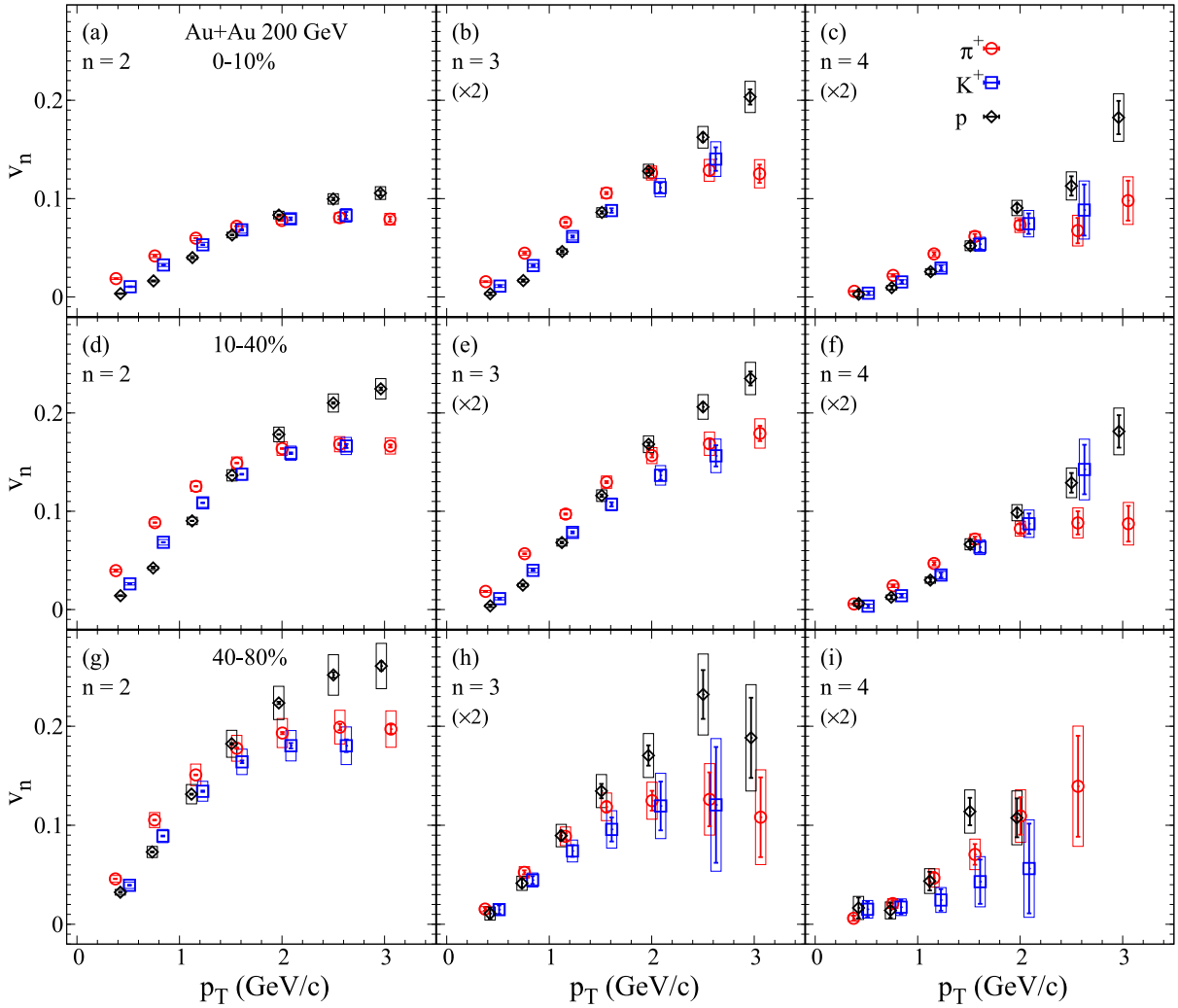

FIG. 3. The transverse-momentum dependence of the identified particle v_2, v_3, and v_4 for 0–10%, 10–40%, and 40–80% central Au+Au collisions at $\sqrt{s_{NN}} = 200$ GeV.

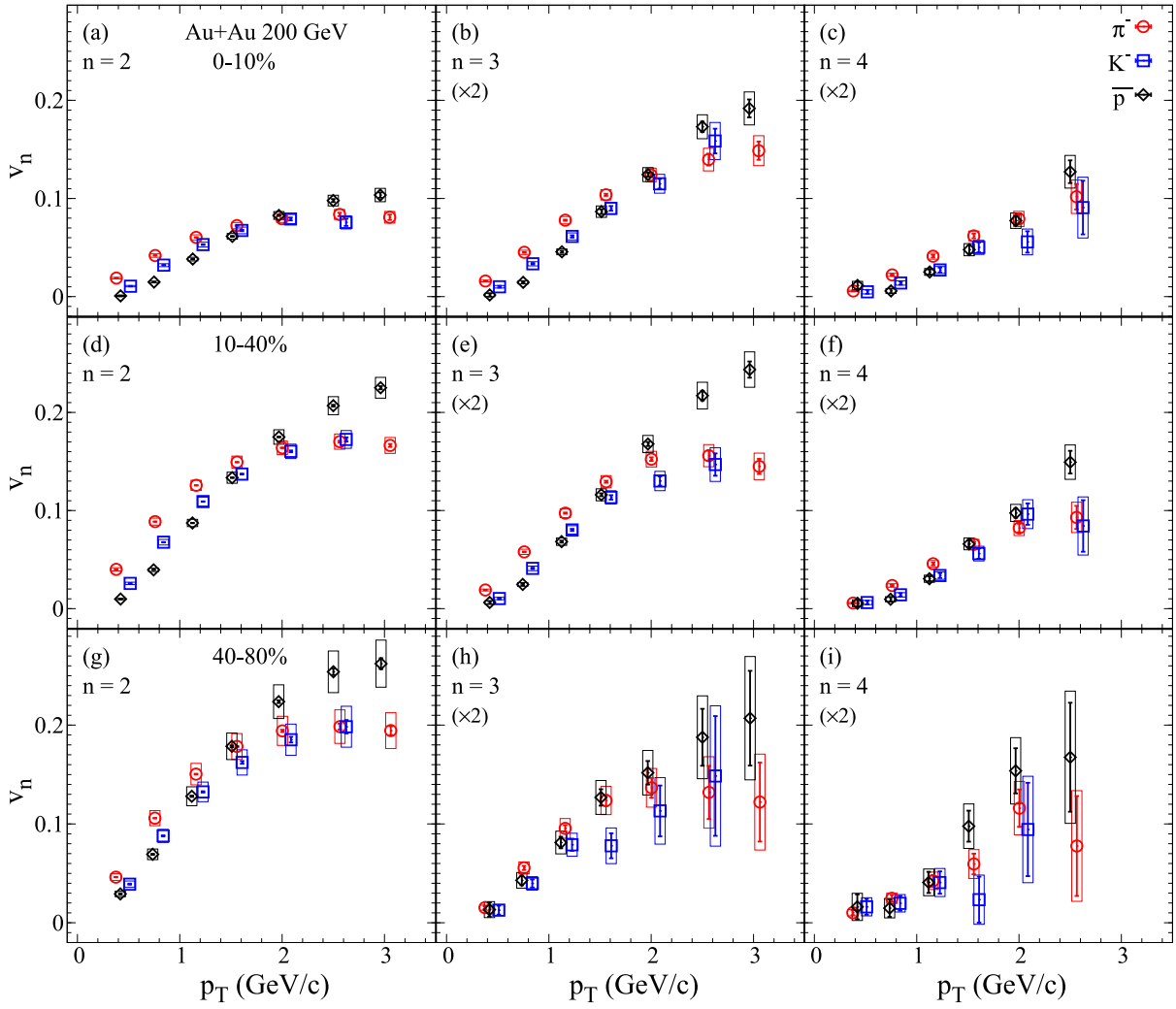

FIG. 4. The transverse-momentum dependence of the identified antiparticle v_2, v_3, and v_4 for 0–10%, 10–40%, and 40–80% central Au+Au collisions at $\sqrt{s_{NN}} = 200$ GeV.

points. The track-cuts systematic uncertainty ranges from 1% to 3% from central to peripheral collisions. The systematic uncertainty correlated with the nonflow correlations due to Bose-Einstein correlations, resonance decays, and the fragments of individual jets is evaluated by varying the pseudorapidity gap, $\Delta\eta = \eta_1 - \eta_2$, for the track pairs used in the measurement. The variation of the results for $\Delta\eta$ values of 0.6 and 0.8 was studied. The systematic uncertainty from the nonflow correlations ranges from 2% to 5% from central to peripheral collisions. The systematic uncertainty from varying the particle identification cuts about their nominal values [41] ranges from 1% to 3% from central to peripheral collisions. The overall systematic uncertainty, considering all sources as independent of each other, was evaluated via the quadrature sum of the uncertainties from the individual cut variations. They range from 3% to 7% from central to peripheral collisions.

IV. RESULTS AND DISCUSSION

The v_n results for Au+Au collisions at 200 GeV are shown as a function of the transverse momentum in Sec. IV A, kinetic energy in Sec. IV B, and centrality in Sec. IV C. The statistical uncertainties are shown as the straight vertical lines, while the point-by-point systematic uncertainties are shown as the open boxes.

A. v_n as a function of transverse momentum

The panels (a)–(c) of Fig. 1 present the particle and antiparticle v_2, v_3, and v_4 for 0–80% central Au+Au collisions at $\sqrt{s_{NN}} = 200$ GeV. The measurements show clear similarities in the values and trends between the particle and antiparticle. A more quantitative conclusion can be made by forming the differences Δv_2, Δv_3, and Δv_4, which are shown in panels (d)–(i). The Δv_2 [41], Δv_3, and Δv_4 values for pions and kaons indicate little if any difference between positive and negative mesons of the same species. Although the Δv_3 and Δv_4 show little if any difference between protons and antiprotons, the Δv_2 is nonzero, with a value of $0.0028 \pm 0.0002(\text{stat}) \pm 0.0003(\text{syst})$. As pointed out in our prior studies [73,74], the v_n difference between positive and negative particles could be accounted for by considering nu-

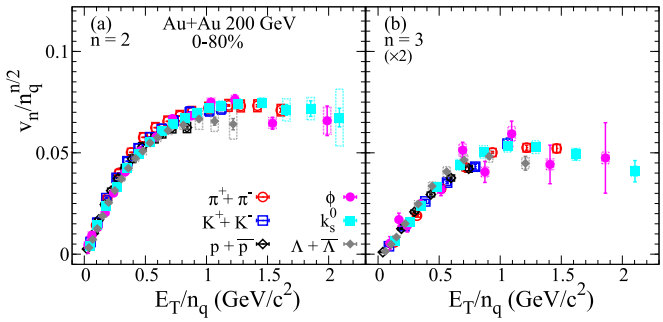

FIG. 5. The scaled identified particle elliptic and triangular flow vs the scaled transverse kinetic energy for 0–80% central Au+Au collisions at $\sqrt{s_{NN}} = 200$ GeV.

clear stopping power which decreases with increasing $\sqrt{s_{NN}}$. Such an effect is expected to be small at $\sqrt{s_{NN}} = 200$ GeV.

Figure 2 shows the transverse-momentum dependence at midrapidity of v_2 (a) and v_3 (b) of π, K, p, Λ, φ, and K_s^0, and of v_4 (c) of π, K, and p for 0–80% central Au+Au collisions at $\sqrt{s_{NN}} = 200$ GeV. The measurements indicate similar increasing then flattening trends as a function of p_T in $v_{n=2,3,4}(p_T)$ for all particles shown. Also mass ordering at low p_T is observed for v_2, v_3, and v_4. The shapes of the flow harmonics for light and strange mesons are comparable, which suggests similar flow strength for u, d, and s quarks.

The p_T dependence of v_2, v_3, and v_4 for π, K, p and their charge conjugates are shown in Figs. 3 and 4. The measurements indicate mass ordering at low p_T for v_2, v_3, and v_4. Our measurements are in good agreement with the prior measurements [32,49,75]. The v_2 values are found to be higher in peripheral collisions (40–80% centrality) compared to those in central collisions (0–10% centrality). The v_3 and v_4 values indicate a weak centrality dependence. This observation is compatible with the picture in which the viscous effects reduce the initial spatial anisotropic effects on the higher-order flow harmonics [7,76].

B. Scaled v_n as a function of scaled kinetic energy

Prior investigations [48,74] have indicated that particle species dependence remains in plots of v_n vs p_T when each

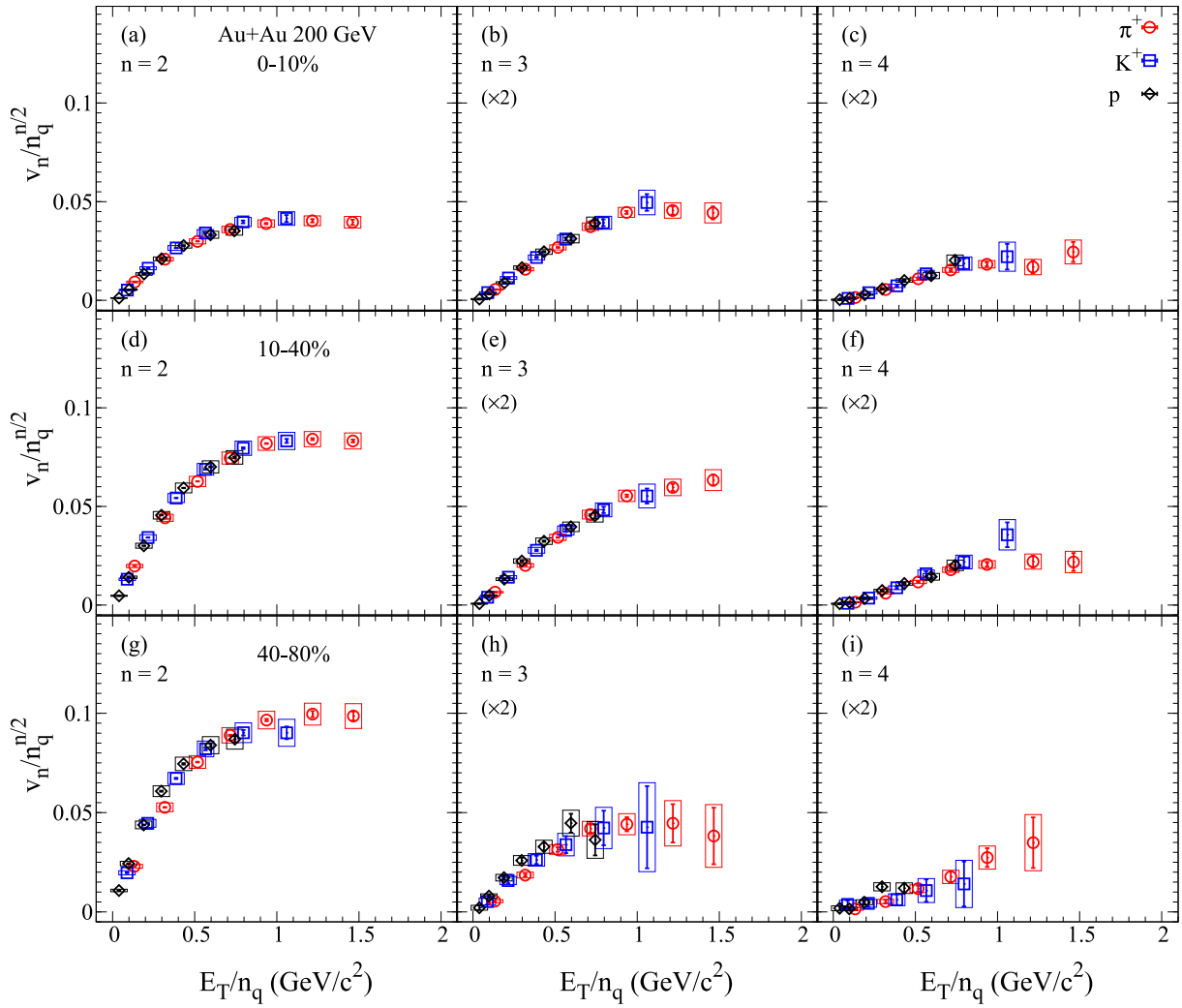

FIG. 6. The scaled identified particle v_2, v_3, and v_4 vs the scaled transverse kinetic energy for 0–10%, 10–40%, and 40–80% central Au+Au collisions at $\sqrt{s_{NN}} = 200$ GeV.

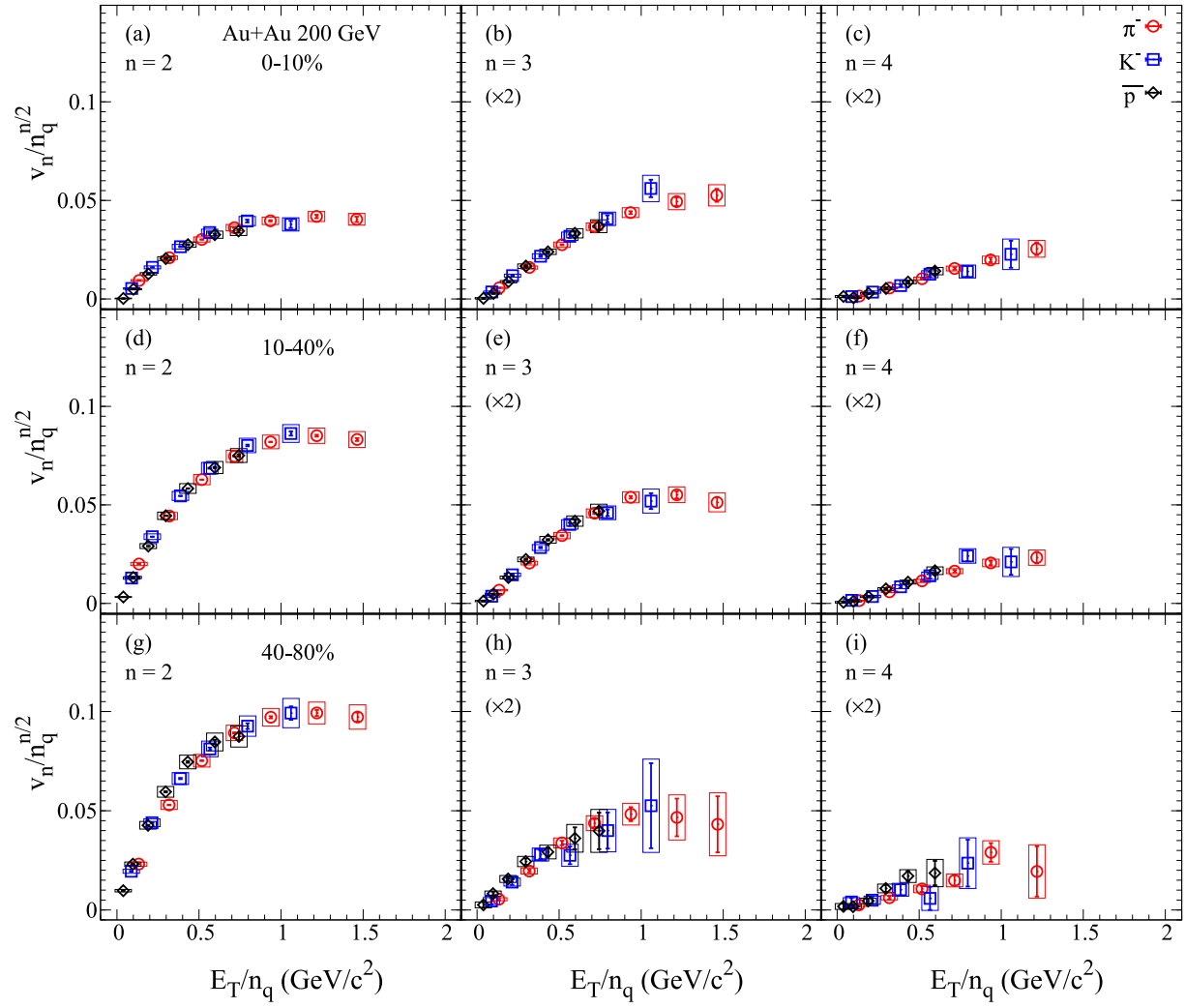

FIG. 7. The scaled identified antiparticle v_2, v_3, and v_4 vs the scaled transverse kinetic energy for 0–10%, 10–40%, and 40–80% central Au+Au collisions at $\sqrt{s_{NN}} = 200$ GeV.

are scaled by the number of constituent quarks, n_q. The breakdown of this scaling is also shown for the present data in the Appendix. A modified scaling function of $v_n/n_q^{n/2}$ vs scaled kinetic energy ($E_T = m_T - m_0$ and $m_T = \sqrt{p_T^2 + m_0^2}$) is suggested to work better, and will be tested in this work.

Figure 5 shows the number-of-constituent-quark (n_q) scaled v_2 (a) and v_3 (b) as a function of scaled kinetic energy dependence at midrapidity ($|y| < 1.0$) of π, K, p, Λ, φ and K_s^0 for 0–80% central collisions. The measurements indicate a clear scaling for the $v_n/n_q^{n/2}$ vs scaled kinetic energy E_T/n_q [43] at the top RHIC energy of $\sqrt{s_{NN}} = 200$ GeV. The observed scaling properties of v_2 and v_3 imply that the measured collective flow develops during the partonic phase. The NCQ scaling properties of these data can be further explored via the centrality dependence of v_n vs the scaled kinetic energy. Figures 6 and 7 show the scaled kinetic energy dependence of v_2, v_3, and v_4 for π^+, K^+, p and for π^-, K^-, $\bar{p}$ at midrapidity ($|y| < 1.0$) of 0–10%, 10–40%, and

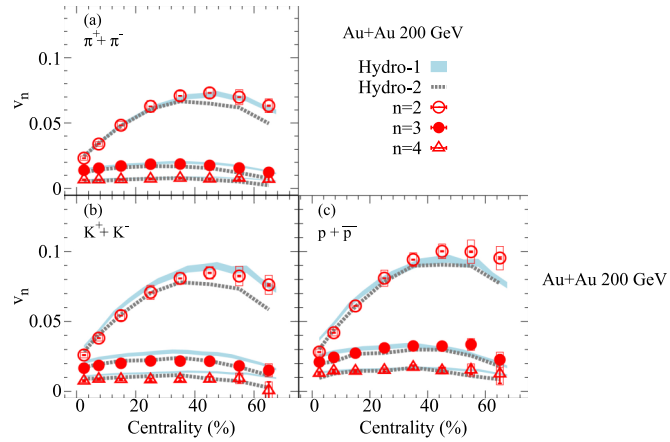

FIG. 8. The centrality dependence of the π, K, and p_T integrated v_2, v_3, and v_4 values for $p_T < 2.0$ GeV/c in Au+Au collisions at $\sqrt{s_{NN}} = 200$ GeV. The solid and dashed lines represent the two hydrodynamic models used here [54,55].

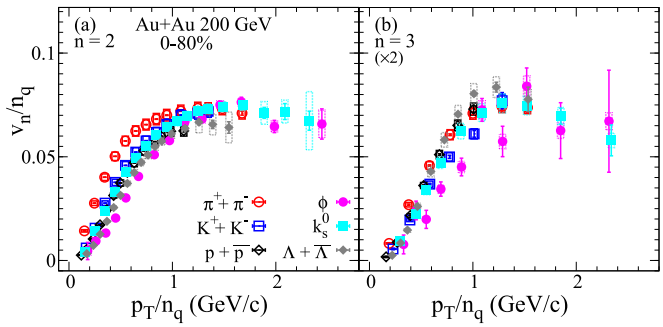

FIG. 9. The scaled identified particle elliptic and triangular flow vs the scaled p_T for 0–80% central Au+Au collisions at $\sqrt{s_{NN}} = 200$ GeV.

40–80% central Au+Au collisions. The measurements indicate a scaling of the $v_n/n_q^{n/2}$ vs E_T/n_q [43] for all the centrality intervals shown. Such measurements could add constraints to theoretical models attempting to reproduce the anisotropic flow.

C. v_n as a function of centrality and comparison with models

The centrality dependence of the p_T-integrated v_2, v_3, and v_4 of π, K, and p for Au+Au collisions at $\sqrt{s_{NN}} = 200$ GeV are presented in Fig. 8. The flow harmonics show a characteristic dependence on the collision centrality that reflects the interplay between initial-state effects and the final-state effects from central to peripheral collisions [15,25,26,77–84]. In addition, the v_n values decrease with increasing harmonic order. Such an observation reflects the increase of viscous effects with increasing harmonic order [26]. The weakening centrality dependence for higher flow harmonic, especially v_3, is caused by the dominating geometry fluctuations.

Thorough comparisons between data and theoretical calculations are carried out for all harmonics v_2, v_3, and v_4. The shaded bands in Fig. 8 indicate two viscous hydrodynamic model predictions [54,55], which are summarized in Table I. Note that these two models differ in their initial- and final-state assumptions. However, both models show qualitative agreement with the present measurements. The predictions from Hydro-1 (cf. Table I) give a closer description of the measured v_2 values. The Hydro-1 model overpredicts the kaon

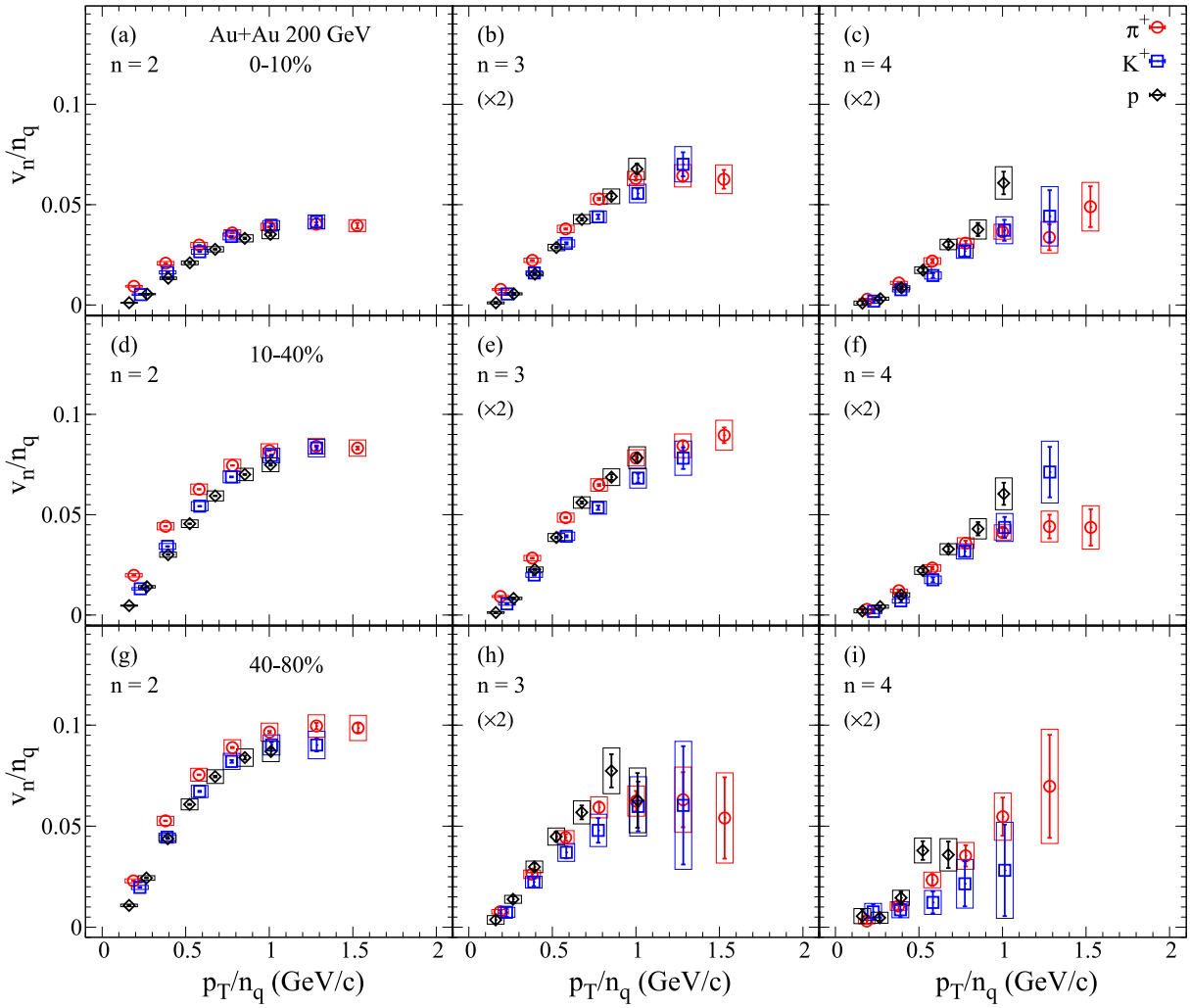

FIG. 10. The scaled identified particle v_2, v_3, and v_4 vs the scaled p_T for 0–10%, 10–40%, and 40–80% central Au+Au collisions at $\sqrt{s_{NN}} = 200$ GeV.

v_3 and v_4 values. The Hydro-2 model gives a closer description to the v_3 and v_4 values.

V. SUMMARY

In summary, we have presented new differential measurements of v_2, v_3, and v_4, at midrapidity for identified hadrons as a function of centrality and transverse momentum in Au+Au collisions at $\sqrt{s_{NN}} = 200$ GeV. The p_T-differential measurements indicate a sizable centrality and mass-order dependence for the measured flow harmonics. The similarities of the shapes of the v_n vs p_T curves for light and strange mesons indicate that the heavier s quarks flow as strongly as the lighter u and d quarks. We also observed number-of-constituent-quark scaling for v_2, v_3, and v_4, which suggests that the measured collective flow develops during the partonic phase. Furthermore, a qualitative agreement between the present flow measurements and the two viscous hydrodynamic calculations was obtained. These comparisons may provide additional constraints on the transport properties of the medium produced in these collisions.

ACKNOWLEDGMENTS

We thank the RHIC Operations Group and RCF at BNL, the NERSC Center at LBNL, and the Open Science Grid consortium for providing resources and support. This work was supported in part by the Office of Nuclear Physics within the U.S. DOE Office of Science, the U.S. National Science Foundation, National Natural Science Foundation of China, Chinese Academy of Science, the Ministry of Science and Technology of China and the Chinese Ministry of Education, the Higher Education Sprout Project by Ministry of Education at NCKU, the National Research Foundation of Korea, Czech Science Foundation and Ministry of Education, Youth and Sports of the Czech Republic, Hungarian National Research, Development and Innovation Office, New National Excellency Programme of the Hungarian Ministry of Human Capacities, Department of Atomic Energy and Department of Science and Technology of the Government of India, the National Science Centre of Poland, the Ministry of Science, Education and Sports of the Republic of Croatia, German Bundesministerium für Bildung, Wissenschaft,

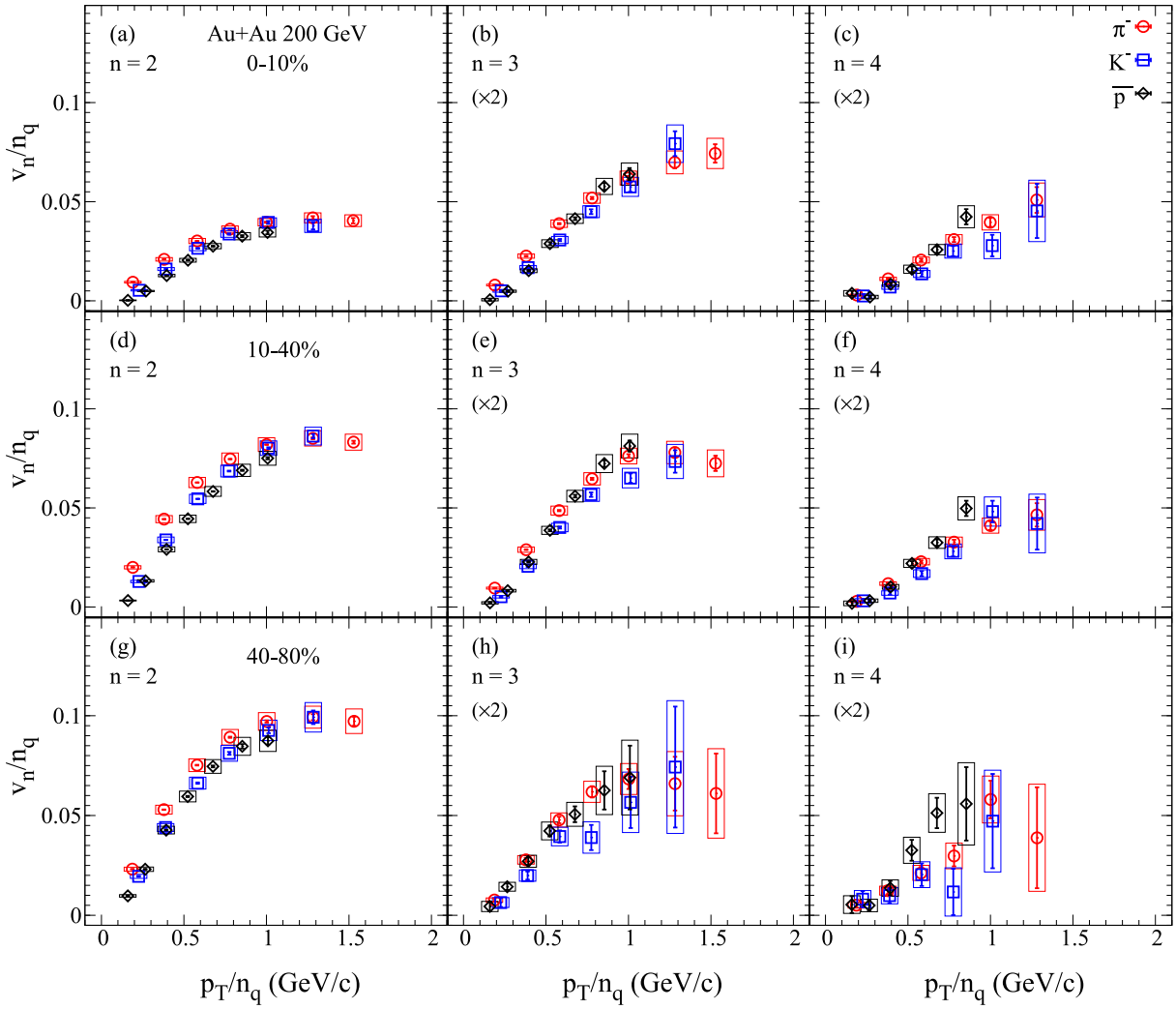

FIG. 11. The scaled identified antiparticle v_2, v_3, and v_4 vs the scaled p_T for 0–10%, 10–40%, and 40–80% central Au+Au collisions at $\sqrt{s_{NN}} = 200$ GeV.

Forschung and Technologie (BMBF), Helmholtz Association, Ministry of Education, Culture, Sports, Science, and Technology (MEXT), and Japan Society for the Promotion of Science (JSPS).

APPENDIX: SCALED v_n AS A FUNCTION OF SCALED p_T

The number-of-constituent-quark scaling [48,49,85] can be employed to show the collective flow was generated at the partonic level. In the number-of-constituent-quark scaling process, at a given p_T hadrons are created from n_q quarks with transverse momentum p_T/n_q. Figures 9–11 presents v_n/n_q of different particle species as a function of p_T/n_q. The number-of-constituent-quark scaled v_n as a function of p_T/n_q seems to show a global tendency for all particles species, although there are small differences for each v_n.

[1] E. V. Shuryak, Phys. Lett. B **78**, 150 (1978).
[2] E. V. Shuryak, Phys. Rep. **61**, 71 (1980).
[3] B. Muller, J. Schukraft, and B. Wyslouch, Annu. Rev. Nucl. Part. Sci. **62**, 361 (2012).
[4] P. Danielewicz, R. A. Lacey, P. B. Gossiaux, C. Pinkenburg, P. Chung, J. M. Alexander, and R. L. McGrath, Phys. Rev. Lett. **81**, 2438 (1998).
[5] K. H. Ackermann *et al.* (STAR Collaboration), Phys. Rev. Lett. **86**, 402 (2001).
[6] F. G. Gardim, F. Grassi, M. Luzum, and J.-Y. Ollitrault, Phys. Rev. Lett. **109**, 202302 (2012).
[7] R. A. Lacey, D. Reynolds, A. Taranenko, N. N. Ajitanand, J. M. Alexander, F.-H. Liu, Y. Gu, and A. Mwai, J. Phys. G: Nucl. Part. Phys. **43**, 10LT01 (2016).
[8] K. Adcox *et al.* (PHENIX Collaboration), Phys. Rev. Lett. **89**, 212301 (2002).
[9] U. W. Heinz and P. F. Kolb, Nucl. Phys. A **702**, 269 (2002).
[10] T. Hirano, U. W. Heinz, D. Kharzeev, R. Lacey, and Y. Nara, Phys. Lett. B **636**, 299 (2006).
[11] P. Huovinen, P. F. Kolb, U. W. Heinz, P. V. Ruuskanen, and S. A. Voloshin, Phys. Lett. B **503**, 58 (2001).
[12] T. Hirano and K. Tsuda, Phys. Rev. C **66**, 054905 (2002).
[13] P. Romatschke and U. Romatschke, Phys. Rev. Lett. **99**, 172301 (2007).
[14] M. Luzum, J. Phys. G: Nucl. Part. Phys. **38**, 124026 (2011).
[15] H. Song, S. A. Bass, U. Heinz, T. Hirano, and C. Shen, Phys. Rev. Lett. **106**, 192301 (2011); **109**, 139904(E) (2012).
[16] J. Qian, U. W. Heinz, and J. Liu, Phys. Rev. C **93**, 064901 (2016).
[17] B. Schenke, S. Jeon, and C. Gale, Phys. Lett. B **702**, 59 (2011).
[18] D. Teaney and L. Yan, Phys. Rev. C **86**, 044908 (2012).
[19] N. Magdy, P. Parfenov, A. Taranenko, I. Karpenko, and R. A. Lacey, Phys. Rev. C **105**, 044901 (2022).
[20] N. Magdy, X. Sun, Z. Ye, O. Evdokimov, and R. Lacey, Universe **6**, 146 (2020).
[21] J. Adam *et al.* (STAR Collaboration), Phys. Lett. B **809**, 135728 (2020).
[22] N. Magdy (STAR Collaboration), EPJ Web Conf. **171**, 16002 (2018).
[23] N. Magdy and R. A. Lacey, Phys. Lett. B **821**, 136625 (2021).
[24] N. Magdy (STAR Collaboration), Nucl. Phys. A **982**, 255 (2019).
[25] N. Magdy, O. Evdokimov, and R. A. Lacey, J. Phys. G: Nucl. Part. Phys. **48**, 025101 (2020).
[26] J. Adam *et al.* (STAR Collaboration), Phys. Rev. Lett. **122**, 172301 (2019).
[27] N. Magdy, J. Phys. G: Nucl. Part. Phys. **49**, 015105 (2022).
[28] S. Voloshin and Y. Zhang, Z. Phys. C **70**, 665 (1996).
[29] A. M. Poskanzer and S. A. Voloshin, Phys. Rev. C **58**, 1671 (1998).
[30] J. Adams *et al.* (STAR Collaboration), Phys. Rev. Lett. **95**, 122301 (2005).
[31] L. Adamczyk *et al.* (STAR Collaboration), Phys. Rev. C **94**, 034908 (2016).
[32] L. Adamczyk *et al.* (STAR Collaboration), Phys. Rev. Lett. **116**, 062301 (2016).
[33] J. Adams *et al.* (STAR Collaboration), Phys. Rev. C **72**, 014904 (2005).
[34] J. Adams *et al.* (STAR Collaboration), Phys. Rev. Lett. **92**, 052302 (2004).
[35] T. Hirano, U. W. Heinz, D. Kharzeev, R. Lacey, and Y. Nara, Phys. Rev. C **77**, 044909 (2008).
[36] S. Singha and M. Nasim, Phys. Rev. C **93**, 034908 (2016).
[37] S. A. Voloshin, Nucl. Phys. A **715**, 379c (2003).
[38] D. Molnar and S. A. Voloshin, Phys. Rev. Lett. **91**, 092301 (2003).
[39] R. J. Fries, V. Greco, and P. Sorensen, Annu. Rev. Nucl. Part. Sci. **58**, 177 (2008).
[40] B. H. Alver, C. Gombeaud, M. Luzum, and J.-Y. Ollitrault, Phys. Rev. C **82**, 034913 (2010).
[41] L. Adamczyk *et al.* (STAR Collaboration), Phys. Rev. C **88**, 014902 (2013).
[42] J. Adam *et al.* (ALICE Collaboration), J. High Energy Phys. 09 (2016) 164.
[43] L. X. Han, G. L. Ma, Y. G. Ma, X. Z. Cai, J. H. Chen, S. Zhang, and C. Zhong, Phys. Rev. C **84**, 064907 (2011).
[44] B. Abelev *et al.* (STAR Collaboration), Phys. Rev. Lett. **99**, 112301 (2007).
[45] B. Abelev *et al.* (STAR Collaboration), Phys. Rev. C **81**, 044902 (2010).
[46] B. Abelev *et al.* (STAR Collaboration), Phys. Rev. C **75**, 054906 (2007).
[47] S. A. Voloshin, A. M. Poskanzer, and R. Snellings, in *Relativistic Heavy Ion Physics*, edited by R. Stock, Landolt-Börnstein, New Series, Vol. 23 (Springer, Berlin, 2010), p. 293.
[48] L. Adamczyk *et al.* (STAR Collaboration), Phys. Rev. C **98**, 014915 (2018).
[49] A. Adare *et al.* (PHENIX Collaboration), Phys. Rev. C **93**, 051902 (2016).
[50] C.-J. Zhang and J. Xu, Phys. Rev. C **93**, 024906 (2016).
[51] R. A. Lacey, A. Taranenko, N. N. Ajitanand, and J. M. Alexander, arXiv:1105.3782.

[52] S. Acharya *et al.* (ALICE Collaboration), J. High Energy Phys. 09 (2018) 006.
[53] S. Acharya *et al.* (ALICE Collaboration), J. High Energy Phys. 06 (2020) 147.
[54] P. Alba, V. Mantovani Sarti, J. Noronha, J. Noronha-Hostler, P. Parotto, I. Portillo Vazquez, and C. Ratti, Phys. Rev. C **98**, 034909 (2018).
[55] B. Schenke, C. Shen, and P. Tribedy, Phys. Rev. C **99**, 044908 (2019).
[56] J. S. Moreland, J. E. Bernhard, and S. A. Bass, Phys. Rev. C **92**, 011901(R) (2015).
[57] B. Schenke, P. Tribedy, and R. Venugopalan, Phys. Rev. Lett. **108**, 252301 (2012).
[58] S. A. Bass *et al.*, Prog. Part. Nucl. Phys. **41**, 255 (1998).
[59] M. Bleicher *et al.*, J. Phys. G: Nucl. Part. Phys. **25**, 1859 (1999).
[60] K. Ackermann *et al.* (STAR Collaboration), Nucl. Instrum. Methods Phys. Res., Sect. A **499**, 624 (2003).
[61] M. Anderson *et al.*, Nucl. Instrum. Methods Phys. Res., Sect. A **499**, 659 (2003).
[62] W. J. Llope *et al.*, Nucl. Instrum. Methods Phys. Res., Sect. B **241**, 306 (2005).
[63] Y.-F. Xu, J.-H. Chen, Y.-G. Ma, A.-H. Tang, Z.-B. Xu, and Y.-H. Zhu, Nucl. Sci. Technol. **27**, 126 (2016).
[64] W. J. Llope *et al.*, Nucl. Instrum. Methods Phys. Res., Sect. A **759**, 23 (2014).
[65] B. Alver, M. Baker, C. Loizides, and P. Steinberg, arXiv:0805.4411.
[66] L. Adamczyk *et al.* (STAR Collaboration), Phys. Rev. C **86**, 054908 (2012).
[67] A. Bilandzic, R. Snellings, and S. Voloshin, Phys. Rev. C **83**, 044913 (2011).
[68] A. Bilandzic, C. H. Christensen, K. Gulbrandsen, A. Hansen, and Y. Zhou, Phys. Rev. C **89**, 064904 (2014).
[69] K. Gajdošová (ALICE Collaboration), Nucl. Phys. A **967**, 437 (2017).
[70] J. Jia, M. Zhou, and A. Trzupek, Phys. Rev. C **96**, 034906 (2017).
[71] I. Selyuzhenkov and S. Voloshin, Phys. Rev. C **77**, 034904 (2008).
[72] J. Barrette *et al.* (E877 Collaboration), Phys. Rev. C **56**, 3254 (1997).
[73] L. Adamczyk *et al.* (STAR Collaboration), Phys. Rev. Lett. **110**, 142301 (2013).
[74] L. Adamczyk *et al.* (STAR Collaboration), Phys. Rev. C **93**, 014907 (2016).
[75] B. I. Abelev *et al.* (STAR Collaboration), Phys. Rev. C **77**, 054901 (2008).
[76] B. Schenke, P. Tribedy, and R. Venugopalan, Phys. Rev. C **89**, 064908 (2014).
[77] P. Liu and R. A. Lacey, Phys. Rev. C **98**, 021902(R) (2018).
[78] H. Niemi, G. S. Denicol, H. Holopainen, and P. Huovinen, Phys. Rev. C **87**, 054901 (2013).
[79] F. G. Gardim, J. Noronha-Hostler, M. Luzum, and F. Grassi, Phys. Rev. C **91**, 034902 (2015).
[80] J. Fu, Phys. Rev. C **92**, 024904 (2015).
[81] H. Holopainen, H. Niemi, and K. J. Eskola, Phys. Rev. C **83**, 034901 (2011).
[82] G.-Y. Qin, H. Petersen, S. A. Bass, and B. Muller, Phys. Rev. C **82**, 064903 (2010).
[83] Z. Qiu and U. W. Heinz, Phys. Rev. C **84**, 024911 (2011).
[84] C. Gale, S. Jeon, B. Schenke, P. Tribedy, and R. Venugopalan, Phys. Rev. Lett. **110**, 012302 (2013).
[85] M. Abdallah *et al.* (STAR Collaboration), Phys. Rev. C **103**, 064907 (2021).